The Compensatory CO_2 Fertilization and Stomatal Closure Effects on Runoff Projection in the Western United States

Xue-Yan Zhang[1], Jiming Jin[2], Xubin Zeng[1], Wuchao Yang[3], Charles P. Hawkins[2,4], Antônio A. M. Neto[1], and Guo-Yue Niu[1]

[1]Department of Hydrology and Atmospheric Sciences, The University of Arizona, Tucson, AZ, USA

[2]Department of Watershed Sciences, Utah State University, Logan, UT, USA

[3]College of Natural Resources and Environment, Northwest A&F University, Yangling, Shaanxi, China

[4]The Ecology Center and National Aquatic Monitoring Center, Utah State University, Logan, UT, USA

Corresponding author:

Guo-Yue Niu (niug@email.arizona.edu)

† Department of Hydrology and Atmospheric Sciences

1133 E. James E. Rogers Way

JW Harshbarger Bldg (#11), Room 318D

PO Box 210011

Tucson AZ 85721-0011

Key Points:

- Annual runoff of the major Western US rivers is projected to decline significantly by 2099 under RCP8.5.
- The counteracting CO_2 fertilization and stomatal closure effects, as significant as the warming effect, are roughly compensatory.
- Due to the two offsetting CO_2 effects, warming remains the dominant driver for the projected runoff decline at river basin scales.

Abstract

Water availability in the dry Western United States (US) under a warming climate and increasing water use demand has become a serious concern. Previous studies have projected future runoff changes across the Western US but ignored the impacts of ecosystem response to elevated CO_2 concentration. Here, we aim to understand the impacts of elevated CO_2 on future runoff changes through ecosystem responses to both rising CO_2 and associated warming using the Noah-MP model with representations of vegetation dynamics and plant hydraulics. We first validated Noah-MP against observed runoff, LAI, and terrestrial water storage anomaly from 1980–2015. We then projected future runoff with Noah-MP under downscaled climates from three climate models under RCP8.5. The projected runoff declines variably from the Pacific Northwest by –11% to the Lower Colorado River basin by –92% from 2016–2099. To discern the exact causes, we conducted an attribution analysis of two additional sensitivity experiments: one with constant CO_2 and another with monthly LAI climatology based on the Penman-Monteith equation. Results show that surface "greening" (due to the CO_2 fertilization effect) and the stomatal closure effect are the second largest contributors to future runoff change, following the warming effect. These two counteracting CO_2 effects are roughly compensatory, leaving the warming effect to remain the dominant contributor to the projected runoff declines at large river basin scales. This study suggests that both surface "greening" and stomatal closure effects are important factors and should be considered together in water resource projections.

Plain Language Summary:

Water shortage in the Western United States (US) is becoming increasingly serious due to increasing socioeconomic demands and global warming. Although previous studies have projected various degrees of runoff changes, they neglect the impact of rising CO_2 on runoff projections. To explore the possible role of CO_2 that may play in the hydrologic cycle, we conducted three experiments with the newly improved Noah-MP land model including vegetation dynamics and plant hydraulics. Consistent with previous studies, the Western US tends to be drier toward the end of the 21st Century. CO_2-induced LAI increases (surface "greening") contribute considerably to the projected widespread transpiration increases and runoff reductions; however, these changes are nearly compensated by the stomatal closure effect of CO_2 on transpiration, leaving the warming effect to remain the major cause to these transpiration and runoff changes. Therefore, the dual roles of CO_2 in the hydrologic cycle through interactions with vegetation processes need to be considered in water resource projections.

1 Introduction

Water availability in the dry Western United States (US) under increasing water demands and a warming climate has become a serious concern. Expanding population, high total water use rate, and rapidly growing agriculture in the Western US, have posed a great challenge on sustainable management of water resources (Anderson and Woosley, 2006). Besides, restoration of endangered riparian ecosystems related to depleted water resources, which has recently received an increasing attention, requires more water in the episodes of droughts (Anderson and Woosley, 2006). In addition to substantial water demands, significant reductions in annual runoff have been observed across the Western US due to climate change (Forbes et al., 2018), with earlier snowmelt runoff and reduced summer flows (Clow, 2010; Hamlet et al., 2007). It is crucial to discern the controlling factors of runoff for reducing the uncertainties in future runoff and water resource projections.

Runoff generation is largely affected by static factors of soil property and topography and changes in climate and associated ecosystem response. Changing precipitation patterns, such as amounts as well as intensity, duration, and frequency, directly affect runoff generation. Rising temperatures enhance evaporation through increases in the atmospheric water demand and induce a greater loss of snow mass with a shrinking snow cover, causing a positive feedback to the warming (Milly and Dunne, 2020). Terrestrial ecosystem plays a key role in the terrestrial hydrologic cycle (Lemordant et al., 2018; Ukkola et al., 2016) through root water uptake, transpiration, canopy interception loss, and hydraulic redistribution. Recent studies, however, show conflicting results. Singh et al. (2020) suggested that increases in leaf area index (LAI) and plant water use efficiency (WUE) due to elevated CO_2 result in an insignificant trend in the observed runoff in the Southeastern US during 1951–2015. Y Yang et al. (2016) reported minor changes in LAI and leaf-level transpiration under elevated CO_2 in 18 tropical forest catchments over 1982–2010 based on *in situ* and satellite observations. Yet, Frank et al. (2015) found CO_2-induced increases in plant WUE cannot nullify increases in transpiration caused by increases in LAI and temperature across the European forests during the 20th century. Ukkola et al. (2016) suggested that the projected runoff reductions caused by changing climate may be moderated (exacerbated) because of reduced (increased) vegetation growth in wet and humid (dry) Australia. Although consistent temperature increases and slight precipitation changes are projected for the Western US (Easterling et al., 2017; Vose et al., 2017), whether the vegetation response to elevated CO_2 and associated climate change alleviate or aggravate the future water shortage over the already dry Western US remains unknown.

Raw runoff outputs from Earth system models (ESMs) is not generally used in regional hydrologic projections. The coarse horizontal resolution of ESMs (~100 km) poorly characterizes the heterogeneity in the soil, vegetation, and topographic characteristics. The low spatial resolution may result in uncertainties of the water balance in hydrologic projections that may already miss key hydrologic processes in current ESMs, such as soil water-groundwater interactions and subsurface lateral flows (Fan et al., 2019; Sun et al., 2016). More importantly, current land surface models (LSMs) used in ESMs do not adequately represent ecosystem resilience, producing an unrealistically decreasing LAI trend in most drying drylands (Mao et al., 2013). During droughts, these models produces unrealistically low rain use efficiency (biomass productivity per unit rainfall) (Ma et al., 2017; Zhu et al., 2019). Inadequate representations of plant and root hydraulics, especially under a changing climate, may result in low transpiration and high runoff. Most recent models have started to implement plant hydraulics (Kennedy et al.,

2019; Li et al., 2021; Niu et al., 2020; S Zhu et al., 2017) and explicitly represent plant water storage supplied by dynamic root water uptake and groundwater capillary rise to enhance ecosystem resilience to drought stress (Niu et al., 2020).

A commonly-used way to project future water availability is to use offline LSMs driven by downscaled ESM's atmospheric outputs (Hamlet and Lettenmaier, 1999; Naz et al., 2016; Sun et al., 2016). Hamlet and Lettenmaier (1999) used a "delta" method to perturb historical climate data by mapping spatially averaged future changes in precipitation and temperature resulting from global climate models (GCMs) relative to their historical records. They reported that the annual runoff of the Columbia River Basin in 2045 would be 85–110% of that of 1961–1997. Naz et al. (2016) projected an increase in runoff in spring and winter but widespread summer runoff declines in the mid-century (2011–2050) compared to the baseline period (1966–2005) with the VIC hydrological model driven by the downscaled and high-resolution precipitation and temperature from ten climate models of the Fifth Phase of the Coupled Model Intercomparison Project (CMIP5) under the Representative Concentration Pathway (RCP) 8.5. Sun et al. (2016) projected more than 20% annual runoff declines in the central part of the Western US during 2031–2060 compared to that during 1979–2007, except in the Lower Colorado River basin. However, these previous studies considered only the impacts of temperature and precipitation but neglected the impacts of other forcing variables including downward longwave radiation and specific humidity that show an apparent trend and thus may directly affect the projected evapotranspiration (ET) and runoff trends (Figure S1). Also, these studies neglected the significant rise of CO_2 and related ecohydrological consequences.

A widespread surface "greening" over the boreal forests has been observed and attributed to the CO_2 fertilization effect under a warming climate (Z Zhu et al., 2017). Also, despite a drying trend (Chang et al., 2020), arid and semiarid ecosystems have been greening as evidenced from pronounced greenness increases (Fensholt et al., 2012), large-scale woody encroachment (Andela et al., 2013), and enhanced net carbon sinks (Ahlström et al., 2015) over global drylands. Z Zeng et al. (2018) reported that vegetation greening has contributed to over 50% of global ET increases during the past three decades. However, plant stomatal closure and increased WUE caused by elevated CO_2 concentration may result in less transpiration at the leaf level scale (Field et al., 1995). The CO_2 inhibition effect on stomatal opening is widely used in interpreting runoff changes projected by ESMs with the conceptual Penman-Monteith & Budyko framework (Milly and Dunne, 2016; Y Yang et al., 2019). Therefore, the model projected future runoff change may be largely controlled by the relative importance of these two counteracting CO_2 effects to terrestrial ecosystem responses, whereas the surface "greening" induced by CO_2 fertilization effects is greatly affected by model representations of ecosystem resilience to increasing drought stress (Niu et al., 2020).

In this study, we aim to discern the dominant processes controlling the projected future runoff changes using the Noah-MP LSM (Niu et al., 2011) with explicit representations of vegetation dynamics and plant hydraulics (Niu et al., 2020). Here, our specific objectives are to 1) project future runoff changes in the Western US; 2) quantify the impacts of LAI changes (or "greening") and stomatal closure on ET changes using the Penman-Monteith (PM) equation; 3) investigate the role of the two counteracting effects of CO_2 ("greening" and stomatal closure) playing in the hydrologic cycle. We first performed future projections of runoff and factors influencing runoff generation in the Western US under the RCP 8.5 scenario with Noah-MP. We then conducted an attribution analysis on the modeling results based on the PM equation (Y

Yang et al., 2019) and isolated the two counteracting CO_2 effects on the projected changes in ET and runoff through model sensitivity experiments with constant CO_2 concentration and static leaf dynamics.

2 Materials and Methods

2.1 Data

2.1.1 Forcing, Vegetation, and Soil Data

We used the Phase 2 of the North American Land Data Assimilation System (NLDAS-2) atmospheric forcing data (Xia et al., 2012) to drive Noah-MP during the historical period from 1980 through 2015. This dataset spans from January 1979 to present at a resolution of 0.125° with an hourly time step throughout the contiguous US (CONUS). NLDAS-2 includes downward shortwave and longwave radiation fluxes, surface air pressure and temperature, specific humidity, wind speed, and precipitation rate. NDLAS-2 has been widely verified and employed in modeling studies over the CONUS domain (Ma et al., 2017; Xia et al., 2012). We used the global 1-km hybrid State Soil Geographic Database and the USGS 24-category vegetation data, which were resampled to fit the NLDAS-2 resolution to determine the dominant soil and vegetation types (for use in Noah-MP) over the Western US in both the historical and future simulations.

We used the CMIP5 climate models' output (Taylor et al., 2012) for future projections. Nonlinear yearly CO_2 concentration (Prather et al., 2013) was used to represent future CO_2 changes (Figure S2). We selected the model outputs from three CMIP5 GCMs experiments under RCP 8.5 because they provide sub-daily atmospheric variables for driving Noah-MP, including GFDL-ESM2G (at 2.0°×2.5°), MIROC5 (1.4°×1.4°), and IPSL-CM5A-MR (1.3°×2.5°). The three models represent divergent future climate changes, where the most aggressive increase in air temperature occurs in IPSL-CM5A-MR (Buotte et al., 2019), and the least temperature increase in GFDL-ESM2G (Figure S1). We downscaled these 3-hourly data (except precipitation) to the resolution of NLDAS-2 through bilinear interpolation and corrected the biases of the downscaled data using linear regression models by retaining the probability distributions of historical values similar to those of NLDAS-2 (Dettinger et al., 2004). The daily precipitation data (Abatzoglou, 2013) from the selected GCMs were interpolated to a spatial resolution of 0.125° by bilinear interpolation and disaggregated into a temporal resolution of 3 hours following the method described by Buotte et al. (2019). This method first calculates the ratio of the 3-hourly CMIP5 precipitation to the daily CMIP5 precipitation total and then disaggregated the Multivariate Adaptive Constructed Analogs daily precipitation product based on these ratios over each grid cell. Through downscaling and bias-corrections, the biases in these GCM outputs are largely reduced for the historical period (Figure S1), enhancing the credibility of the future projections.

2.1.2 Observational Data

To calibrate and evaluate the Noah-MP's performance, we used ground-based runoff, satellite-derived LAI and terrestrial water storage (TWS) change, upscaled FLUXNET data of gross primary production (GPP) and ET using model tree ensemble (FLUXNET MTE), and ground-based snow water equivalent data (SWE) developed at the University of Arizona (UA) (Broxton et al., 2016; Dawson et al., 2017; X Zeng et al., 2018). We calibrated and validated the

simulated runoff during 1980–2015 against the USGS WaterWatch monthly runoff data at two-digital hydrological unit code (HUC2) basins (Rivers 14–18). This runoff dataset is generated using stream gage observations, the corresponding drainage basins, and HUC2 boundaries (Brakebill et al., 2011), which has been taken as a surrogate of natural streamflow (Ashfaq et al., 2013; Ma et al., 2017). We selected a consistent and continuous LAI product to evaluate the simulated LAI, which is an improved product (Yuan et al., 2011) of the Moderate-Resolution Imaging Spectroradiometer (MODIS) LAI at a spatial resolution of 1 km and a temporal resolution of 8 days. We upscaled this LAI dataset into the resolution of NLDAS-2 (0.125°) and aggregated it into a monthly product during 2002–2015.

Because of high uncertainties related to current ET products (Mueller et al., 2011), we indirectly evaluated ET simulations using the terrestrial water storage anomaly (TWSA) anomaly derived from gravity changes detected by the Gravity Recovery and Climate Experiment (GRACE) twin satellites. We applied the gain factors to three 1° monthly GRACE TWSA product and averaged these datasets for the period of 2003–2015 to reduce their noises because of various resolutions (Landerer and Swenson, 2012; Sakumura et al., 2014). The FLUXNET MTE dataset is generated by upscaling water, CO_2, and energy fluxes measured at FLUXNET sites, which are densely located in the US, and incorporating remote sensing, meteorological, and land cover data through a machine learning approach (Jung et al., 2011).We downscaled the 0.5° GPP and ET of FLUXNET MTE to 0.125° to assess the modelled GPP and ET. The daily UA SWE product is developed using *in situ* observations and 4-km gridded PRISM precipitation and temperature data and has been a benchmark for large-scale SWE evaluations (Broxton et al., 2016; Cho et al., 2020). We reprocessed the daily SWE data into a spatial resolution of 0.125° and a temporal resolution of monthly to evaluate the simulated SWE.

2.2 Model

We used Noah-MP (Niu et al., 2011), a widely-used LSM that simulates the exchanges of energy, water, and carbon between the terrestrial ecosystem and the atmosphere. The model includes one canopy layer, up to three snow layers depending on the snow depth, four soil layers with a total depth of 2 m, and an unconfined aquifer. Noah-MP represents surface heterogeneity with a "semi-tile" scheme that separately computes the energy, water, and carbon fluxes for vegetated and bare fractions of a model grid cell (Niu et al., 2011). Surface runoff and subsurface runoff are parameterized as functions of water table depth based on the TOPMODEL concept.

Noah-MP adopts the simple bucket-type groundwater model of Niu et al. (2007) to represent groundwater recharge into the aquifer (or "bucket") in wet periods and groundwater capillary rise from the "bucket" during dry periods. It also introduces a scaling factor, f_{mic}, (between 0 and 1; fraction of micropore volume) to reduce the capillary rise to account for the presence of subsurface macropores and thus helps improve the modeled soil moisture variability in the State of Illinois (Z L Yang et al., 2011). In general, a larger f_{mic} produces a wetter soil with smaller soil moisture variabilities. In this study, we used a constant f_{mic} of 0.3 for all experiments over the Western US. The hydraulic conductivity of the aquifer is parameterized as a harmonic average of those of the bottom soil layer and the water table. Groundwater capillary rise is demonstrated important for plants to survive drought stress over the central US basins (Niu et al., 2020).

Noah-MP incorporates a simple but efficient dynamic vegetation model (Niu et al., 2011). This model explicitly represent photosynthesis, carbon allocation, respiration, turnover,

and leaf death due to temperature and water stresses (Dickinson et al., 1998; Niu et al., 2011; Parton et al., 1978). Noah-MP calculates the gross photosynthesis rate, *A*, as a sum of leaf-level gross photosynthesis rate, A_i (μmol CO_2 m^{-2} s^{-1}; i = 1, 2 for sunlit and shaded leaves per unit leaf area, respectively), weighted by sunlit and shaded LAI. The leaf-level A_i is calculated as the minimum of three limiting carboxylation rates: the light-limited rate, the Rubisco-limited rate, and the limitation by the transport of photosynthate for C_3 and C_4 plants (Collatz et al., 1992; Farquhar et al., 1980). Noah-MP represents the leaf-level stomatal conductance, $g_{s,i}$ and A_i under the control of abiotic factors, such as atmospheric humidity and CO_2 concentration, c_a, for sunlit and shaded leaves (Ball et al., 1987):

$$g_{s,i} = g_0 + m\frac{A_i}{c_s}\frac{e_s}{e_i}P_{atm} \quad (1)$$

where c_s is CO_2 concentration at the leaf surface (Pa) controlled by intermittent turbulent diffusion of c_a through the leaf boundary layer: $c_s = c_a - \frac{A_i P_{atm}}{1.37 r_b}$, where r_b is the leaf boundary layer resistance; e_s and e_i are the water vapor pressure at the leaf surface and the saturated vapor pressure inside the leaves (Pa) at leaf surface temperature, respectively; g_0 is the minimum conductance (μmol m^{-2} s^{-2}); m is the slope constant of the $g_{s,i} - A_i$ relationship; P_{atm} is the atmospheric pressure (Pa). Because A_i for the light-limited and Rubisco-limited rates of C_3 plants and transport-limited rate of C_4 plants is linked to the intercellular CO_2 concentration, $c_i = c_a - \frac{A_i P_{atm}}{1.37 r_b + 1.65/g_{s,i}}$, Noah-MP iteratively solves the above equation with a first guess of c_i = 0.7 c_a for C_3 plants and c_i = 0.4 c_a for C_4 plants. Because $g_{s,i}$ is inversely related to c_s, a higher c_s due to elevated c_a results in a reduction in $g_{s,i}$ and subsequently a reduction in leaf-level transpiration, inducing a "stomatal closure" effect on transpiration. On the other hand, A_i increases with increasing c_i controlled by the diffusion of c_a through the leaf boundary layer and plant stomata. LAI increases with increasing assimilated carbon (A_i), resulting in a "surface greening" effect on transpiration.

Reduction in A_i due to soil water stress is parameterized through the control of plant water availability, β, on the optimum carboxylation rate at 25°C. The Noah-MP version used in this study also includes a dynamic root submodule that explicitly describes plant water storage supplied by dynamic root water uptake through hydrotropic root growth to meet the transpiration demand (Niu et al., 2020). The plant water availability factor β controlling A_i and $g_{s,i}$ is parameterized as a function of water storage in the living plant tissues, M_q (Niu et al., 2020):

$$\beta = min\left(1.0, \frac{M_q - M_{q,wilt}}{M_{q,max} - M_{q,wilt}}\right) \quad (2)$$

where $M_{q,wilt}$ represents the minimum plant water storage at the wilting point of 30 bar (306 m or 3.0 MPa), and $M_{q,max}$ the maximum plant water storage when the plants are at full hydration. $M_q - M_{q,wilt}$ is the plant water available for transpiration, and ($M_{q,max} - M_{q,wilt}$) is the maximum water that a plant can lose through transpiration until its wilting point. M_q is depleted by transpiration while supplied by root water uptake, which is further controlled by root surface area that is converted from root biomass at each layer and the water pressure gradient between the soils and the roots. Compared to the static root in previous versions of Noah-MP, the current version greatly improve plant drought resilience through hydrotropic root growth and groundwater capillary rise in the central US (Niu et al., 2020).

2.3 Model Experiments

We conducted two sets of simulations using Noah-MP with the parameterization schemes including all recent improvements (Table S1): a historical simulation from 1980–2015 using the NLDAS-2 forcing and projections from 2016–2019 driven by the downscaled climatic forcing. The historical simulation, starting with arbitrary initial states and a constant CO_2 concentration of 360 ppm, is spun up for seven times from 1980 through 2015 (mainly for TWS anomaly), and the last loop is used for analysis. The future projections were performed with the downscaled and bias-corrected forcing data from 2016–2099. The initial conditions for future projections were from the last loop of the historical simulation of Noah-MP driven by downscaled GCM outputs during 1980–2015. In this study, we selected the RCP 8.5 scenario because the CO_2 effects are more apparent with the highest CO_2 growth rate.

In the set of future projections, we conducted three experiments: 1) using Noah-MP with the RCP 8.5 CO_2 concentration (hereafter CTRL); 2) based on CTRL but with the constant CO_2 of 1980 concentration (CON-CO_2); and 3) based on CTRL but with the monthly LAI climatology of MODIS LAI (from 2002–2015) (STATIC-LAI; DVEG = 1). These three experiments are designed to discern the surface greening effect and stomatal closure effect: CTRL includes both effects; STATIC-LAI removes the greening effect but retains the stomatal closure effect; and CON-CO_2 excludes the stomatal closure effects and significantly reduces the LAI trends compared with those in CTRL (to be discussed later in Section 3.4).

To evaluate Noah-MP modeled runoff, LAI, TWSA, GPP, ET, and SWE, we calculated the relative bias (RB), Pearson Correlation coefficient (r), Nash-Sutcliffe efficiency (NSE), and linear trends between simulations and observations using USGS WaterWatch runoff, MODIS LAI, GRACE TWSA, FLUXNET MTE, and UA SWE datasets across the Western US, respectively. For the projection results, we calculated long-term linear trends of annual runoff, LAI, transpiration, and ET during 2016–2099 and examined the significance of these trends using the nonparametric Mann-Kendall test. We also analyzed the contribution of net radiation (R_n), vapor pressure deficit (vpd), surface resistance (r_s), aerodynamic resistance (r_a), and the slope of the saturation vapor pressure–temperature relationship (δ) to the projected ET changes using the PM equation (see Appendix). More importantly, we isolated the contribution of the surface greening and stomatal closure effects through the difference between the model experiments using the PM equation.

3 Results

3.1 Model Evaluation

The modeled runoff is comparable with the USGS WaterWatch runoff data from 1980 through 2015 over the five HUC2 rivers (Figure 1). The RB, r, and NSE values are less than 15%, above 0.89, and over 0.76 for most regions, respectively. The relatively large RB of 47% and low NSE of 0.51 for the Lower Colorado are due mainly to the overestimated NLDAS-2 precipitation (Ma et al., 2017). Noah-MP well reproduces the observed declining trends in runoff, despite slight overestimations of the observed decreases in most rivers. The simulated LAI agrees with the observed monthly LAI during 2002–2015 for each river in terms of mean, timing, and variance, with RB values of less than 13%, r values of over 0.92, and NSE values of over 0.73, although Noah-MP slightly overestimates LAI variabilities and thus results in a negative NSE in the Lower Colorado (Figure 2). Both the simulated and observed LAI values do

not exhibit apparent trends in all rivers, due possibly to the non-significant change in CO_2 concentration during this short period (2002–2015).

We also compared the simulated monthly TWSA with GRACE TWSA during 2003–2015 (Figure 3). The simulated monthly TWSA is derived by subtracting the monthly mean of the simulated TWS during 2004–2009 to be consistent with the procedure of the GRACE TWSA products. Here, the modeled TWS is the sum of SWE, soil moisture, groundwater storage, canopy water, and the plant water storage. The simulated TWSA agrees well with GRACE in phase and variability in most rivers, with the r and NSE values being above 0.81 and 0.29, respectively. Promisingly, Noah-MP captures well the observed TWSA trends, except in the Upper Colorado, suggesting that ET was also well simulated. Noah-MP also showed comparable estimations of ET and GPP with those of FLUXNET MTE and of SWE with those of UA SWE over each river basin, respectively (Figure S3–S5). Overall, the good agreement between the simulated and the observed runoff, LAI, TWSA, and relevant variables ensures an improved credibility of Noah-MP for projected future runoff and vegetation changes.

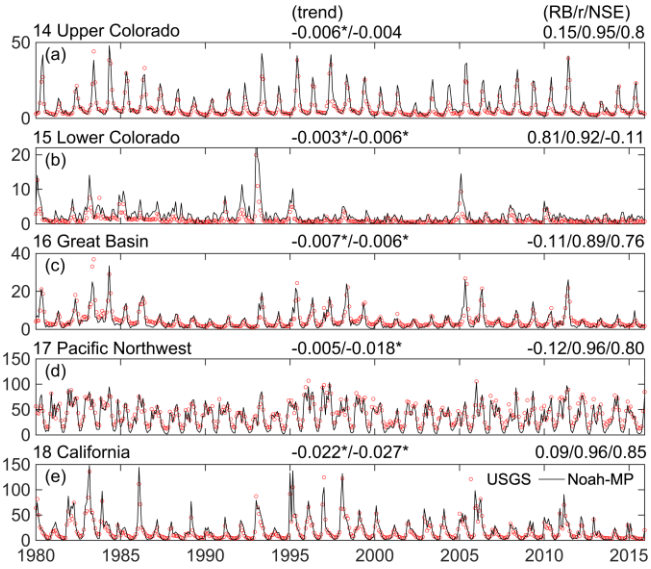

Figure 1. The Noah-MP simulated and observed monthly runoff during 1980–2015 of the HUC2 river basins in the Western US (unit: mm): (a) the Upper Colorado (River 14), (b) the Lower Colorado (River 15), (c) the Great Basin (River 16), (d) the Pacific Northwest (River 17), and (e) California (River 18). Also shown on top of each panel are the linear trend (mm/month) of the observed/modeled and model evaluation metrics in terms of RB/r/NSE. RB = relative bias; r = Pearson correlation coefficient; NSE = Nash-Sutcliffe efficiency.

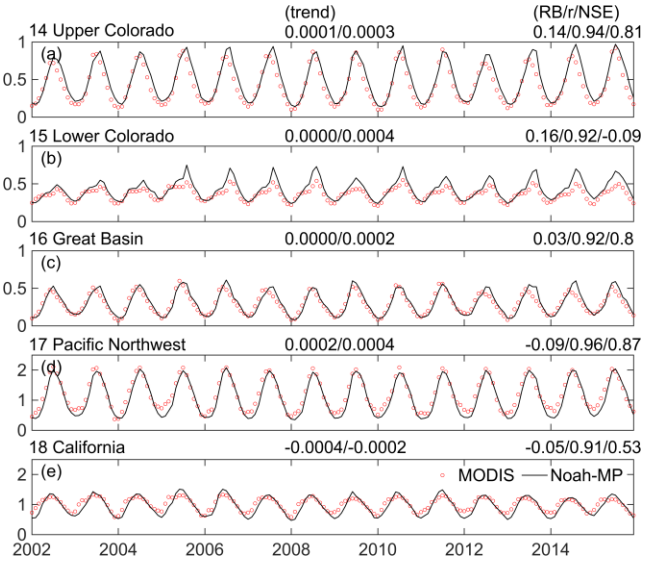

345

346 **Figure 2.** Same as Figure 1 but for monthly LAI during 2002–2015 (unit: m^2/m^2). The trend unit
347 is m^2/m^2/month.

348

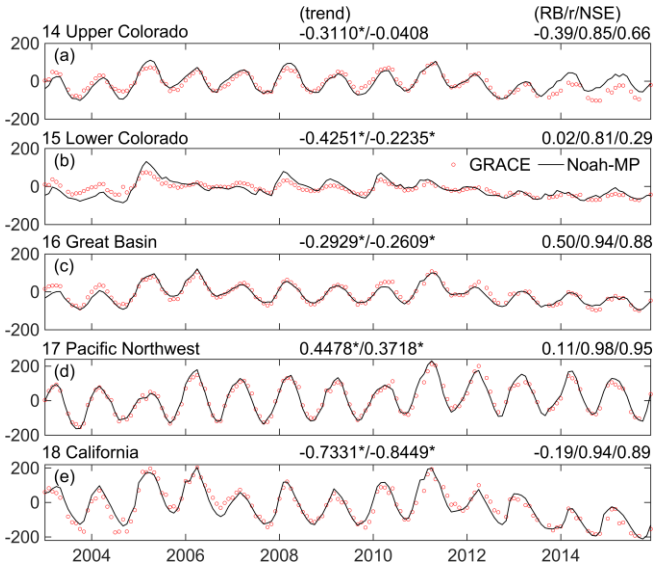

349

350 **Figure 3.** Same as Figure 1 but for monthly TWSA during 2003–2015 (unit: mm). The trend unit
351 is mm/month.

352 3.2 Projected Runoff Changes

353 The Noah-MP projected runoff declines remarkably across the Western US rivers in the
354 future under the different climate produced by the three different GCMs (Figure 4a). The annual
355 mean runoff averaged over these rivers decreases by up to -71% during 2016–2099 (-12
356 mm/decade), -92% (-6 mm/decade), -52% (-5 mm/decade), -11% (-7 mm/decade), and -30% (-
357 13 mm/decade), over River 14 to River 18, respectively. The trends with a unit of percent in this
358 study were calculated as the total linear changes relative to the linear fit of the stating year
359 (2016). The TWS also exhibits substantial decreasing trends at a rate of -134, -152, -104, -2, and

-49 mm/decade over these rivers, respectively (Figure 4c), resulting in deeper water tables because groundwater storage accounts for the majority of TWS. Therefore, the model differences in the annual runoff trends are generally consistent with those in the modeled TWS trends. Insignificant precipitation changes (Figure 4b) and substantial TWS declines indicate that ET changes likely control the future runoff trends for the Western US, based on the annual water balance. However, the decreased annual runoff over the Lower Colorado from IPSL-CM5A-MR and MIROC5 and over the Upper Colorado from IPSL-CM5A-MR result from decreasing precipitation due to the smaller magnitudes of ET decreases (Figure 5). Overall, the runoff reductions in the western US rivers are due mainly to increases in ET, which will be further discussed in the next section.

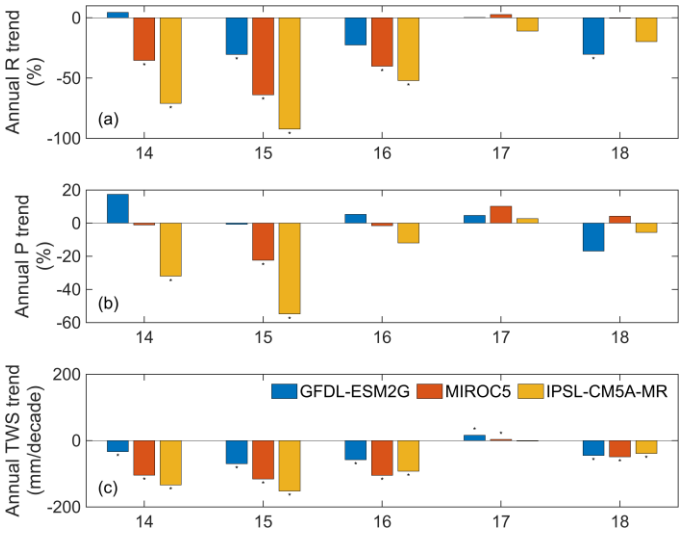

Figure 4. Noah-MP projected (a) runoff change from 2016-2099 (%), (b) precipitation change from 2016-2099 (%), and (c) TWS linear trends (mm/decade) for each river driven by different climates produced by the three GCMs. The asterisks represent significant trends ($p < 0.05$); the linear trends in percent are relative to the starting year of the linear fit (i.e., 2016).

3.3 Projected LAI and ET Changes

From 2016 to 2099, the projected annual mean LAI across the Western US exhibit an increasing trend under all the three climates produced by different GCMs (Figure 5a). The annual LAI increases by 92% (0.06 m^2/m^2/decade), 77% (0.05 m^2/m^2/decade), 101% (0.04 m^2/m^2/decade), 60% (0.08 m^2/m^2/decade), and 57% (0.07 m^2/m^2/decade) over River 14 to River 18, respectively. We will show later that these increasing trends are mainly attributed to the rising CO_2 through comparison with the constant CO_2 experiment (see Section 3.4). Increases in the summer LAI (Figure S6) resulting from IPSL-CM5A-MR are less than those from GFDL-ESM2G due mainly to its relatively high temperatures over the optimum temperature (25°C) for photosynthesis in all the rivers except the relatively colder Pacific Northwest. The differences in LAI changes for other three seasons between 2016–2045 and 2070–2099 are smaller compared to those during summer. Therefore, Noah-MP driven by the GFDL-ESM2G climate with the lowest warming produces the largest annual LAI trends in the Upper and Lower Colorado and Great basin, but the least in the Pacific Northwest, where the vegetation growth is stressed by cold climates.

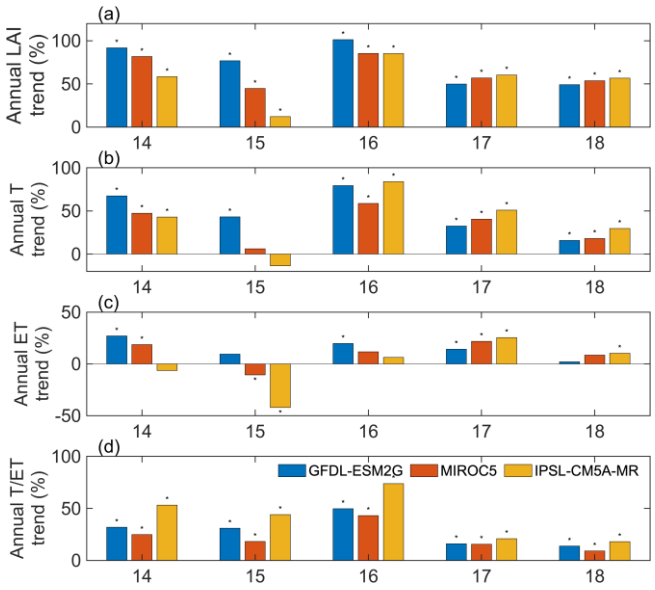

Figure 5. Noah-MP projected trends (represented as percentage change from 2016 to 2099) in annual (a) LAI (leaf area index), (b) transpiration (T), (c) ET (evapotranspiration), and (d) T/ET ratio for the HUC2 rivers. The asterisks represent significant trends ($p < 0.05$).

The annual transpiration (T) is projected to significantly increase across the Western US (Figure 5b). The annual transpiration increases by up to 68% (8 mm/decade), 43% (7 mm/decade), 84% (9 mm/decade), 51% (10 mm/decade), and 30% (8 mm/decade) from 2016 to 2099 over the five HUC2 rivers, respectively. The differences in the projected annual transpiration trends between these rivers are consistent with those of the annual LAI trends, suggesting a strong vegetation phenological impact on transpiration. The projected ET increases by up to 27% (10 mm/decade), 9% (4 mm/decade), 20% (6 mm/decade), 25% (11 mm/decade), and 10% (5 mm/decade) from 2016 to 2099 over the five rivers, indicating that transpiration contributes the most to the ET increases. Additionally, the ratio of transpiration to ET (T/ET) shows a significant increasing trend by up to 53% (2%/decade), 44% (2%/decade), 74% (3%/decade), 21% (1%/decade), and 18% (1%/decade) from 2016 to 2099 over the five rivers, respectively. Despite the declining transpiration trend in the Lower Colorado for IPSL-CM5A-MR, the T/ET ratio shows an increasing trend due to decreases in ET. The increasing trend in the T/ET ratio indicates an enhanced WUE under the increasing CO_2 concentration. Therefore, the greening effect on ET increase and thus runoff reduction can be mainly attributed to the impacts of LAI increase on increases in transpiration under the increasing atmospheric demand (see also Section 3.4).

We conducted an attribution analysis based on the PM equation (see Appendix), which helps discern the dominant factors contributing to changes in ET. The conceptual PM model represents a "big-leaf" (or a single source) evaporating surface, while Noah-MP represents multiple evaporating sources including soil surface evaporation, interception loss, and transpiration. By fitting the Noah-MP modeled ET with the PM model, a single "surface resistance" (r_s in PM) can be derived. As such, r_s represents a combined effect of resistances of the soil surface, leaf boundary layer, and leaf stomata, reflecting the overall water supply from the land surface under the atmospheric water demand.

We first calculated the basin-averaged air temperature, pressure and specific humidity, wind speed, surface roughness length, and sensible and latent heat fluxes. Using these basin-averaged values, we calculated the basin-averaged net radiation (*Rn*), water vapor pressure deficit (*vpd*), the slope of the saturated water vapor pressure against air temperature (δ), and aerodynamic resistance (r_a). The basin-averaged r_s was then derived by fitting the resulting ET from the PM equation with inputs of the basin-averaged *Rn*, *vpd*, δ, and r_a against the basin-averaged model outputs of ET. We then quantified the contributions of changes in *Rn*, *vpd*, δ, r_a, and r_s (ΔRn, Δvpd, $\Delta\delta$, Δr_a, and Δr_s in equation A2) during 2070–2099 averaged over each river basin relative to those during 2016–2045 to the corresponding changes in ET (ΔET in equation A2; Figure 6).

The ET changes reconstructed through the PM equation from CTRL agree well with the modeled outputs with an r^2 value of 0.98 (Figure 6b), indicating an overall excellent fit. The non-perfect match may be caused by the averaging, in space and time, ET and the controlling factors, of which the relationships are nonlinear, as well as the difference between r_a used in PM and the multiple aerodynamic resistances used in Noah-MP. The largest positive contributor to ΔET over all the rivers is Δvpd followed by $\Delta\delta$ due to the nature of the increasing slope of the saturated water vapor pressure against temperature (Figure 6a). ΔR_n also positively contributes to ΔET, and it is due to increased downward longwave radiation (Figure S1), surface "greening"-induced reduction in surface albedo, warming-induced reduction in snow (Figure 7f) (Milly and Dunne, 2020). ΔET due to ΔR_n, Δvpd, and $\Delta\delta$ is the largest for IPSL-CM5A-MR (which produces the strongest warming among the three GCMs), but the lowest for GFDL-ESM2G with a weaker warming, because *vpd* and δ are strongly dependent on temperature. Due to the slightly slowing winds (Figure S1), Δr_a plays a negative but negligible role in the ET changes. Increases in r_s, which may include the combined effects of stomatal closure, surface "greening", and soil surface drying, largely reduce ET by -0.35 (mm/day), -0.71 (mm/day), -0.19 (mm/day), -0.15 (mm/day), and -0.20 (mm/day) over river basins 14–18, respectively, representing the largest negative contributor. Because the negative contribution of Δr_s exceeds the combined positive contribution of other variables, ΔET is negative over the Lower Colorado for MIROC5 (Figure 5c). However, due to the bad fit between the PM-derived and the modeled ET (Figure 6b), this approach fails to explain the ET changes over the Lower Colorado for IPSL-CM5A-MR. From this analysis, it is apparent that Δvpd and Δr_s largely control the future ET changes, suggesting the counteracting effects of the warming-induced increases in the atmospheric demand and the decreasing surface water supply. However, the contribution of Δr_s to ΔET is more complicated due to the soil surface drying and the two counteracting effects of CO_2.

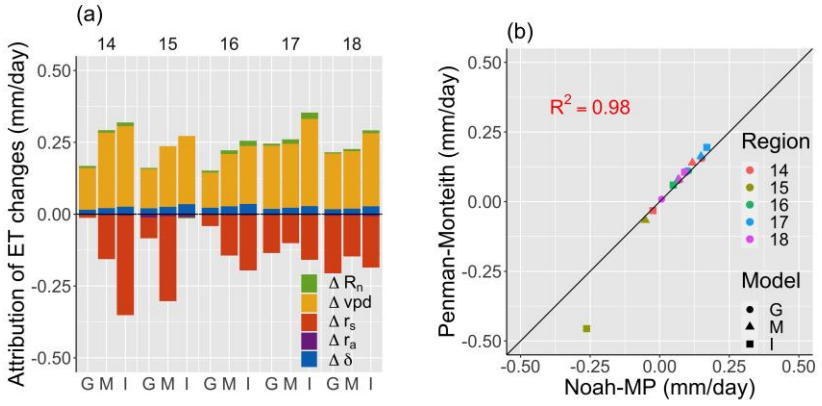

Figure 6. (a) Contribution of ΔR_n, Δvpd, Δr_s, Δr_a, and $\Delta\delta$ to ΔET (2070–2099 relative to 2016–2045); (b) Scatter plot of ΔET during 2070–2099 relative to 2016–2045 resulting from Noah-MP and those computed by the Penman-Monteith equation. G, M, and I represent GFDL-ESM2G, MIROC5, and IPSL-CM5A-MR.

3.4 Compensatory Surface "Greening" and Stomatal Closure Effects

The negative contribution of Δr_s to ΔET can be a combined net effect of plant stomatal closure, surface "greening", and soil surface drying. We assessed the surface "greening" effect through the difference between CTRL and STATIC-LAI and the stomatal closure effect through the difference between CON-CO2 and STATIC-LAI. We first compared some key hydrological variables resulting from CTRL, CON-CO2, and STATIC-LAI over the five rivers (Figure 7) and then conducted a PM-based attribution analysis to quantify the "greening" effect (Figure 8a) and stomatal closure effect (Figure 8b).

STATIC-LAI (without a trend in LAI or "greening" effects) projects a much smaller trend in transpiration (Figure 7b) and ET (Figure 7c) than does CTRL, becoming slightly negative. Consequently, the decreasing runoff trend projected by CTRL is largely reduced due to removal of the "greening" effect in STATIC-LAI. The projected changes in runoff are generally consistent with the changes in TWS (Figure 7e), soil moisture (Figure 7g), and groundwater water storage (Figure 7h), all showing reduced decreasing trends. The comparison between CTRL and STATIC-LAI suggests that the surface "greening" plays an important role in the projected changes of transpiration, ET, runoff, and TWS in the Western US. In addition, STATIC-LAI projects a larger declining trend in SWE (Figure 7f) than does CTRL due likely to less vegetation shading and thus increased solar radiation absorption by the snowpack on the ground.

In CON-CO2, both the "greening" and stomatal closure effects are removed. As a result, the projected LAI trends are largely reduced due to removal of the greening effect. However, CON-CO2 projects a similar level of changes in transpiration (Figure 7b), ET (Figure 7c), runoff (Figure 7d), SWE (Figure 7f), and soil moisture (Figure 7g) to those by CTRL because of the removal of both effects. CON-CO2 projects enhanced runoff reductions in Rivers 17 & 18, because the stomatal closure effect may exceed the impact of surface greening, while Rivers 14–16 showing an opposite case. Because the two counteracting effects of CO_2 are roughly compensatory, CON-CO2 projects changes in the hydrological variables that are comparable with CTRL. This suggests that the warming effect remains the largest factor controlling the long-term change in hydrologic processes.

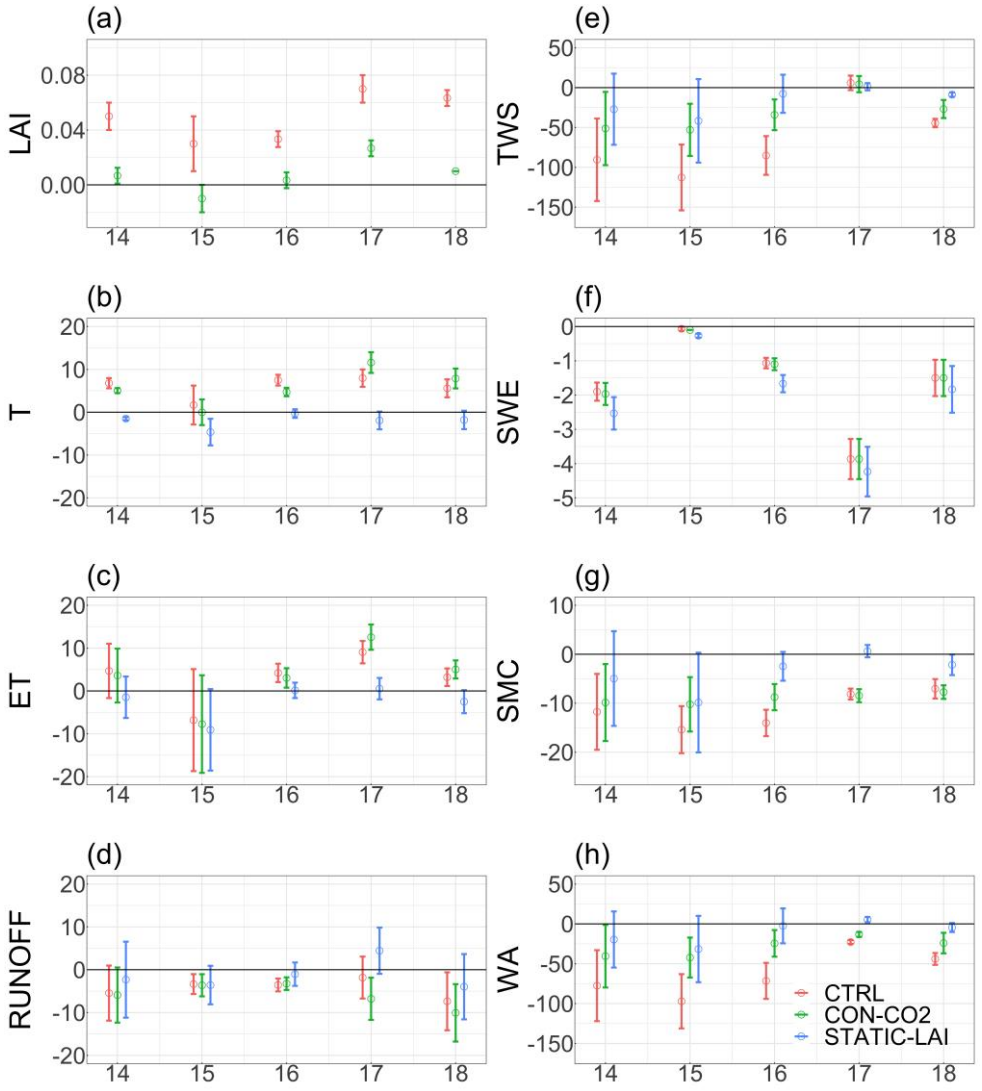

487

488 **Figure 7.** The model projected trends in (a) LAI (m^2/m^2/decade), (b) transpiration (T;
489 mm/decade), (c) evapotranspiration (ET; mm/decade), (d) runoff (mm/decade), (e) terrestrial
490 water storage (TWS; mm/decade), (f) snow water equivalent (SWE; mm/decade), (g) soil
491 moisture (SMC; mm/decade), and (h) groundwater storage (WA; mm/decade) by CTRL, CON-
492 CO2, and STATIC-LAI for each HUC2 rivers. The circles and error bars represent the ensemble
493 mean of trends and ± 1 standard deviation from the three climate models.

494 We conducted the same PM-based analyses of the two sensitivity experiments: STATIC-
495 LAI (Figure S7) and CON-CO2 (Figure S8). We then computed the difference of the ΔET
496 attributions between CTRL and STATIC-LAI (Figure 8a) and that between CON-CO2 and
497 STATIC-LAI (Figure 8b). The effect of Δr_s stands out above all else, becoming the most
498 dominant contributor in both cases, but the former (Figure 8a) indicates the surface greening
499 effect, while the latter (Figure 8b) indicates the stomatal closure effect.

500 Both STATIC-LAI and CTRL are driven by the increasing RCP8.5 CO_2 concentration.
501 The difference between CTRL and STATIC-LAI removes the CO_2 effects on stomatal closure

but retains only the net "greening" effect (Figure 8a). Also, ΔR_n becomes a positive contributor due to the surface greening. Δr_a can be a positive or negative contributor due possibly to different changes in surface roughness length and zero-displacement height associated with a different extent of greening over various basins under various climates. Δvpd and $\Delta\,\delta$ contributions to ΔET are due largely to the smaller first-derivatives of vpd and δ because Δvpd and $\Delta\delta$ are the same in CTRL and STATIC-LAI experiments.

CON-CO2 completely removes the stomatal closure effect and largely removes the surface greening effects, because other factors such as changes in radiation, temperature, and humidity may contribute to the greening (Figure 7a), while STATIC-LAI completely removes the greening effect but contains the stomatal closure effect. So, the difference between CON-CO2 and STATIC-LAI approximates the stomatal closure effect with the greening effect being mostly removed (Figure 8b). The stomatal closure effect also affects the contribution of changes in Δvpd, $\Delta\delta$, Δr_a, and ΔR_n to ΔET, but with a much smaller magnitude compared to that of Δr_s. The magnitudes of the two counteracting CO_2 effects on ET changes are roughly equal (~0.15 mm/day averaged over all basins and climates, Figure 8c), more than half of the contribution of the warming effects to ET changes, which are dominated by Δvpd (~0.2 mm/day; Figure S7) in CON-CO2.

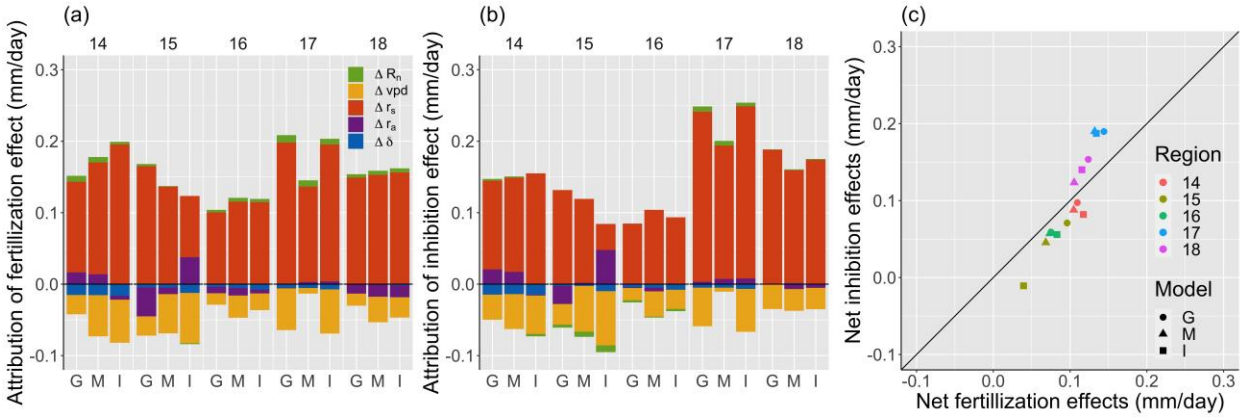

Figure 8. Contribution of ΔR_n, Δvpd, Δr_s, Δr_a, and $\Delta\delta$ to ΔET (2070–2099 relative to 2016–2045). (a) CTRL – STATIC-LAI (surface "greening" effect), (b) CON-CO2 – STATIC-LAI (stomatal closure effect), and (c) the net stomatal closure (or inhibition) effect versus the net surface "greening" (or fertilization) effect over different rivers and under various climates.

4. Discussions

4.1 Projected Runoff and Vegetation Changes

This study was initiated to project future runoff under projected climates following previous studies (e.g., Naz et al., 2016; Sun et al., 2016) but using a different LSM with explicit representations of plant physiological and phenological responses. Overall, the future runoff projected by CTRL declines significantly. Despite the similar conclusions to previous studies, the two sensitivity experiments with Noah-MP reveals the counteracting CO_2 fertilization effects on surface greening and inhibition effects on plant stomatal closure are roughly compensatory. The CON-CO2 experiment is similar to previous studies that did not take CO_2 concentration changes into account. Compared to CTRL, CON-CO_2 projected a similar runoff trend in the

Upper and Lower Colorado and Great Basin but a larger reduction in the Pacific Northwest and California (Figure 7d). In other words, the vegetation responses to elevated CO_2 concentration may alleviate the water shortage in the Pacific Northwest and California. This asymmetric CO_2 effects on the hydrologic cycle (Figure 8c) has also been observed in the Jinghe River basin (Huang et al., 2019) and projected in Australia (Ukkola et al., 2016) in semiarid and semi-humid regions, respectively.

The projected LAI changes are dominated by CO_2 but influenced by multiple other factors, consistent with previous studies (Mahowald et al., 2016; Mankin et al., 2017). Although the LAI trends are substantially reduced due to the removal of increasing CO_2 trend, nonnegligible LAI trends were still found in all regions (except River 15; Figure 7a). Earlier and longer growing season induced by the warming facilitates the CO_2 fertilization effect on the greening, especially over the colder mountain ridges (Figure S9). On the contrary, the warming and precipitation reductions result in decreases in LAI in the warmer Lower Colorado (River 15) without the CO_2 fertilization effects (CON-CO2; Figure S9) This highlights the important control of other abiotic factors on the CO_2 fertilization effects on the long-term trend in vegetation growth. Increasing specific humidity also slightly alleviate the water stress on carbon assimilation, benefiting vegetation growth and reducing forest mortality risks (Liu et al., 2017). Except climatic forcing, plant drought resiliency may also contribute to the projected LAI trends under a drying climate with more frequent droughts. Dynamic root water uptake and groundwater capillary rise may enhance the plant's adaptation capability to changing environments and survive more frequent droughts in the future (Niu et al., 2020). Other model components, such as carbon allocation and respiration schemes (Mankin et al., 2017), may also affect the vegetation greening. Most current LSMs, including Noah-MP, likely overestimate the greening trends due to incomplete understandings of the vegetation processes, such as nutrient limitations and interactions between roots and microbes (Smith et al., 2016).

Since Idso and Brazel (1984), a number of studies have argued the CO_2-induced stomatal closure effects on amelioration of water shortage (Lian et al., 2018; Milly and Dunne, 2016; Roderick et al., 2015; Swann et al., 2016; Y Yang et al., 2019). Our PM-based attribution analyses indicate that stomatal closure due to the CO_2 inhibiting effect can be as large as the warming effect, thereby canceling out the warming effect and resulting in negligible changes in transpiration and ET as shown by STATIC-LAI (Figure 7b & 7c). Although the CO_2-induced stomatal closure remarkably reduces transpiration, widespread runoff reductions (though small) are still projected in the future (Figure 7d), highlighting the importance of warming on the hydrologic cycle as shown by the CON-CO2 experiment. However, surface greening mainly due to rising CO_2 has nonnegligible impacts on the hydrological cycle, equivalent to the stomatal closure effects. Our study suggests that the two complementary CO_2 effects should be considered together rather than emphasizing one of them as done in some previous studies (Idso and Brazel, 1984; Mankin et al., 2019; Milly and Dunne, 2016; Y Yang et al., 2019). Interestingly, the CO_2 fertilization effect on surface greening is lower than the stomatal closure effect at lower elevations (< ~1,500 m) but tends to exceed the stomatal closure effect at higher elevations (> ~1,500 m) (Figure S10). Both grasslands and shrublands tend to exhibit a greater greening effect than the stomatal closure effect at all altitudes (Figures S11 & S12), but the evergreen needleleaf forests show an opposite pattern, more apparently at lower elevations (Figure S13). This is due likely to other abiotic factors (e.g., temperature, humidity, and soil water etc.) that may affect the response of evergreen needleleaf forests to elevated CO_2 concentration, which is worth further studies.

4.2 Uncertainties

In this study, the vegetation types is prescribed during the 100-year simulations under a changing climate. In reality, natural disturbances and human activities may influence the vegetation vigor and species. For example, bark beetle outbreaks and wildfire have resulted in tree mortality in nearly 15% of the forested area across the Western US during the past three decades (Hicke et al., 2016). Tree mortality is also projected to likely increase in the future, especially in the Southwest US (Buotte et al., 2019; Jiang et al., 2013; Thorne et al., 2018). Jiang et al. (2013) projected that half of the regions dominated by evergreen needleleaf forests in the Western US will shift into shrub- and grass-dominant areas by the end of the 21st century under the business-as-usual emission scenario. These potential vegetation changes may increase or reduce runoff by altering the hydrologic cycle (Goeking and Tarboton, 2020). Although the forested area comprises less than 20% of the Western US, future work should better understand the impacts of these disturbances on water resources.

Another source of uncertainties is the T/ET ratio, which is very uncertain due to a lack of direct transpiration observations and thus limited understanding of the vegetation physiological processes. Because of the scarcity of large-scale transpiration observations and accurate ET products, we relied on observational datasets of the USGS monthly runoff and GRACE TWSA, of which the seasonal variations and trends largely represent the cumulative effects of ET, in the calibration. However, Lian et al. (2018) found that the simulated global T/ET ratio by CMIP5 ESMs tends to be lower than *in-situ* observations, indicating that the vegetation would probably play a more important role in future runoff change. They attributed this underestimation to inadequate representations of canopy light use, interception loss, and root water uptake. Noah-MP, like many other LSMs, struggles to simulate a T/ET ratio lower than observations, indicating that the vegetation contribution to ET (Zeng et al., 2017) and thus runoff changes may be underestimated. The low T/ET ratio produced by Noah-MP and other LSMs may be caused by a lack of adequate representations of lateral water flow and water vapor diffusion within the surface soil pores (Chang et al., 2018). Overall, the limited understanding of vegetation dynamics constrains us from better projecting the ecosystem responses to an unprecedent future climate. To reduce these uncertainties, large-scale observations and controlled experiments may be required.

Uncertainties also exist in the validation datasets and downscaling processes. The MODIS LAI product is mainly generated through MODIS reflectance data, a look-up table, and a three-dimensional radiation transfer model (Yan et al., 2016). Uncertainties in the observed LAI tend to be high in regions with dense canopy cover and complex terrain. Therefore, this may explain the relatively high negative model biases in the Pacific Northwest coastal regions and the Cascades. Moreover, the water balance for some grid cells may be not closed because of different sources of validation datasets (Cai et al., 2014; Zheng et al., 2020). For instance, over the Lower Colorado, Noah-MP overestimated both runoff and ET. Additionally, despite the good performance of the linear regression approach in correcting the biases in the CMIP5 data, this method may reduce the interannual variabilities of the variables and usually neglect the dynamic atmospheric processes induced by subgrid variations in topography and land cover (Xue et al., 2014), compared to dynamic downscaling.

5 Conclusions

This study aims to improve the understanding of the impacts of terrestrial ecosystems response to rising CO_2 on terrestrial water resources across the Western US river basins through projections of runoff under different warming climates projected by three GCMs under RCP 8.5. We used the mechanistic Noah-MP LSM with explicit representations of plant physiological and phenological responses to the CO_2 inhibition effect on stomatal opening (stomatal closure) and fertilization effect on photosynthesis (surface "greening"). The good performance of Noah-MP in comparison with observations (Figures 1–3 and Figures S3–S5) gives us some confidence in the projected changes in the 21st Century. Through sensitivity experiments and PM-based attribution analyses, we conclude that:

(1) The projected annual runoff shows a widespread decline over the Upper Colorado, Great Basin, Pacific Northwest, and California by -71%, -52%, -11%, and -30% from 2016-2099, respectively, due mainly to increases in ET, and over the Lower Colorado by -92 % but due mainly to decreases in precipitation.

(2) Both the stomatal closure and surface "greening" effects represent the second largest contributor to the projected increases in ET following the warming effect. The PM-based analysis indicates that the increasing atmospheric demand (through increases in vpd and δ) plays a dominant role over the increasing available energy (through changes in R_n) due to increases in downward longwave radiation, surface "greening" (increases in LAI), and "darkening" (shrinking snow cover).

(3) The two counteracting effects of surface "greening" and stomatal closure are roughly compensatory at the HUC2 river basin scale, and therefore the projected changes in ET and runoff under RCP8.5 (CTRL) show a magnitude of change similar to those with constant CO_2 concentration (CON-CO2) across the Western US HUC2 rivers. However, the strength of the two effects are dependent on vegetation types distributing over different elevation bands, with the stomatal closure effect exceeding the "greening" effect for evergreen needleleaf forests over low elevation bands (< ~1,500 m).

This study suggests that both the surface "greening" and stomatal closure effects are important factors and should be considered together in runoff and water availability projections. In contrast, projections with prescribed LAI seasonal cycle without year-to-year variations (i.e., without the "greening" effect) would lead to misleading results.

Acknowledgments, Samples, and Data

This research project was funded by the NASA MAP Program (80NSSC17K0352), NOAA OAR's OWAQ (NA18OAR4590397), DOE Earth System Modeling Program (DE-AC52-498 07NA27344/B639244), and the Strategic Environmental Research and Development Program (SERDP) of the US Department of Defense awarded to Charles P. Hawkins as the lead Principal Investigator (RC18-1034).

The data used in this study are all available online: NLDAS-2 data (http://www.emc.ncep.noaa.gov/mmb/nldas/); the 1-km hybrid State Soil Geographic Database and the USGS 24-category vegetation data (https://ral.ucar.edu/solutions/products/noah-multiparameterization-land-surface-model-noah-mp-lsm); the monthly USGS Water Watch hydrological unit runoff data (https://waterwatch.usgs.gov/); the FLUXNET-MTE GPP and

latent heat flux data (https://www.bgc-jena.mpg.de/geodb/projects/Home.php); the MODIS LAI data (http://land.sysu.edu.cn/research/data); the GRACE TWSA data (http://grace.jpl.nasa.gov); the University of Arizona SWE data (https://nsidc.org/data/nsidc-0719/versions/1); the CMIP5 model outputs (https://esgf-node.llnl.gov/search/cmip5/); the future CO_2 concentration data under RCP8.5 (https://pcmdi.llnl.gov/mips/cmip5/forcing.html); and the daily precipitation of MACAv2-METDATA (https://climate.northwestknowledge.net/MACA/).

Appendix

We quantified the attribution of ET changes based on the Penman-Monteith equation (Monteith, 1965).

$$\lambda ET = \frac{\delta R_n + \rho_a C_p vpd / r_a}{\delta + \gamma(1 + r_s / r_a)} \quad \text{(A1)}$$

where λ is the latent heat of vaporization (J/kg); ET is the evaporation flux (kg/(m^2/s)); δ is the slope of the saturation vapor pressure-temperature relationship (Pa/K); R_n is the total available energy (equivalent to the sum of sensible and latent heat fluxes; W/m^2); ρ_a is the air density (kg/m^3); C_p is the specific heat of air (J/(kg/K)); vpd is the vapor pressure deficit of the air (Pa); γ is the psychrometric constant (Pa/K); r_a is the aerodynamic resistance (s/m); and r_s is the surface resistance.

The change in ET can be approximated as the sum of ET changes caused by changes in R_n, vpd, r_s, r_a, and δ, following Y Yang et al. (2019), Ban et al. (2020), and Neto et al. (2020):

$$\Delta ET \approx \frac{\partial ET}{\partial R_n}\Delta R_n + \frac{\partial ET}{\partial vpd}\Delta vpd + \frac{\partial ET}{\partial r_s}\Delta r_s + \frac{\partial ET}{\partial r_a}\Delta r_a + \frac{\partial ET}{\partial \delta}\Delta \delta \quad \text{(A2)}$$

where the first derivatives of the five dependent variables in Equation (A2) are as follows:

$$\frac{\partial ET}{\partial R_n} = \frac{\delta}{\gamma[\delta + \gamma(1 + \frac{r_s}{r_a})]} \quad \text{(A3)}$$

$$\frac{\partial ET}{\partial vpd} = \frac{\rho_a C_p}{\lambda r_a[\delta + \gamma(1 + \frac{r_s}{r_a})]} \quad \text{(A4)}$$

$$\frac{\partial ET}{\partial r_s} = \frac{-\gamma[\delta R_n + \frac{\rho_a C_p vpd}{r_a}]}{\lambda r_a[\delta + \gamma(1 + \frac{r_s}{r_a})]^2} \quad \text{(A5)}$$

$$\frac{\partial ET}{\partial r_a} = \frac{\gamma r_s[\delta R_n + \frac{\rho_a C_p vpd}{r_a}]}{\lambda {r_a}^2[\delta + \gamma(1 + \frac{r_s}{r_a})]^2} - \frac{\rho_a C_p vpd}{\lambda {r_a}^2[\delta + \gamma(1 + \frac{r_s}{r_a})]} \quad \text{(A6)}$$

$$\frac{\partial ET}{\partial \delta} = \frac{R_n}{\lambda[\delta + \gamma(1 + \frac{r_s}{r_a})]} - \frac{\delta R_n + \frac{\rho_a C_p vpd}{r_a}}{\lambda[\delta + \gamma(1 + \frac{r_s}{r_a})]^2} \quad \text{(A7)}$$

References

Abatzoglou, J. T. (2013), Development of gridded surface meteorological data for ecological applications and modelling, *Int. J. Climatol.*, *33*(1), 121-131.https://doi.org/10.1002/joc.3413.

Ahlström, A., M. R. Raupach, G. Schurgers, B. Smith, A. Arneth, M. Jung, et al. (2015), The dominant role of semi-arid ecosystems in the trend and variability of the land CO2 sink, *Science*, *348*(6237), 895-899.https://doi.org/10.1126/science.aaa1668.

Andela, N., Y. Liu, A. Van Dijk, R. De Jeu, and T. McVicar (2013), Global changes in dryland vegetation dynamics (1988–2008) assessed by satellite remote sensing: comparing a new passive microwave vegetation density record with reflective greenness data, *Biogeosciences*, *10*(10), 6657-6676.https://doi.org/10.5194/bg-10-6657-2013.

Anderson, M., and L. Woosley (2006), Water availability for the Western United States—Key scientific challenges. Circular 1261, *US Geological Survey, Washington, DC*

Ashfaq, M., S. Ghosh, S. C. Kao, L. C. Bowling, P. Mote, D. Touma, et al. (2013), Near-term acceleration of hydroclimatic change in the western US, *Journal of Geophysical Research: Atmospheres*, *118*(19), 10,676-610,693. https://doi.org/10.1002/jgrd.50816.

Ball, J. T., I. E. Woodrow, and J. A. Berry (1987), A model predicting stomatal conductance and its contribution to the control of photosynthesis under different environmental conditions, in *Progress in photosynthesis research*, edited, pp. 221-224, Springer.

Ban, Z., T. Das, D. Cayan, M. Xiao, and D. P. Lettenmaier (2020), Understanding the Asymmetry of Annual Streamflow Responses to Seasonal Warming in the Western United States, *Water Resources Research*, *56*(12), e2020WR027158.https://doi.org/10.1029/2020WR027158.

Brakebill, J. W., D. M. Wolock, and S. Terziotti (2011), Digital Hydrologic Networks Supporting Applications Related to Spatially Referenced Regression Modeling 1, *JAWRA Journal of the American Water Resources Association*, *47*(5), 916-932.https://doi.org/10.1111/j.1752-1688.2011.00578.x.

Broxton, P. D., N. Dawson, and X. Zeng (2016), Linking snowfall and snow accumulation to generate spatial maps of SWE and snow depth, *Earth and Space Science*, *3*(6), 246-256.https://doi.org/10.1002/2016EA000174.

Buotte, P. C., S. Levis, B. E. Law, T. W. Hudiburg, D. E. Rupp, and J. J. Kent (2019), Near-future forest vulnerability to drought and fire varies across the western United States, *Glob. Chang. Biol.*, *25*(1), 290-303.https://doi.org/10.1111/gcb.14490.

Cai, X., Z. L. Yang, Y. Xia, M. Huang, H. Wei, L. R. Leung, and M. B. Ek (2014), Assessment of simulated water balance from Noah, Noah-MP, CLM, and VIC over CONUS using the NLDAS test bed, *J. Geophys. Res. Atmos.*, *119*(24), 13,751-713,770.https://doi.org/10.1002/2014JD022113.

Chang, L. L., R. Yuan, H. V. Gupta, C. L. Winter, and G. Y. Niu (2020), Why Is the Terrestrial Water Storage in Dryland Regions Declining? A Perspective Based on Gravity Recovery and Climate Experiment Satellite Observations and Noah Land Surface Model With Multiparameterization Schemes Model Simulations, *Water Resources Research*, *56*(11), e2020WR027102.https://doi.org/10.1029/2020WR027102.

Chang, L. L., R. Dwivedi, J. F. Knowles, Y. H. Fang, G. Y. Niu, J. D. Pelletier, et al. (2018), Why do large-scale land surface models produce a low ratio of transpiration to evapotranspiration?, *Journal of Geophysical Research: Atmospheres*, *123*(17), 9109-9130.https://doi.org/10.1029/2018JD029159.

Cho, E., J. M. Jacobs, and C. M. Vuyovich (2020), The value of long-term (40 years) airborne gamma radiation SWE record for evaluating three observation-based gridded SWE data sets by seasonal snow and land cover classifications, *Water resources research*, *56*(1).https://doi.org/10.1029/2019WR025813.

Clow, D. W. (2010), Changes in the timing of snowmelt and streamflow in Colorado: a response to recent warming, *Journal of Climate*, *23*(9), 2293-2306.https://doi.org/10.1175/2009JCLI2951.1.

Collatz, G. J., M. Ribas-Carbo, and J. Berry (1992), Coupled photosynthesis-stomatal conductance model for leaves of C4 plants, *Functional Plant Biology*, *19*(5), 519-538.https://doi.org/10.1071/PP9920519.

Dawson, N., P. Broxton, and X. Zeng (2017), A new snow density parameterization for land data initialization, *Journal of Hydrometeorology*, *18*(1), 197-207.https://doi.org/10.1175/JHM-D-16-0166.1.

Dettinger, M. D., D. R. Cayan, M. K. Meyer, and A. E. Jeton (2004), Simulated hydrologic responses to climate variations and change in the Merced, Carson, and American River basins, Sierra Nevada, California, 1900–2099, *Climatic Change*, *62*(1-3), 283-317.https://doi.org/10.1023/B:CLIM.0000013683.13346.4f.

Dickinson, R. E., M. Shaikh, R. Bryant, and L. Graumlich (1998), Interactive canopies for a climate model, *Journal of Climate*, *11*(11), 2823-2836.https://doi.org/10.1175/1520-0442(1998)011<2823:ICFACM>2.0.CO;2.

Easterling, D. R., J. Arnold, T. Knutson, K. Kunkel, A. LeGrande, L. R. Leung, et al. (2017), Precipitation change in the United States.https://doi.org/10.7930/J0H993CC.

Fan, Y., M. Clark, D. M. Lawrence, S. Swenson, L. Band, S. L. Brantley, et al. (2019), Hillslope hydrology in global change research and Earth system modeling, *Water Resources Research*, *55*(2), 1737-1772.https://doi.org/10.1029/2018WR023903.

Farquhar, G. D., S. v. von Caemmerer, and J. A. Berry (1980), A biochemical model of photosynthetic CO 2 assimilation in leaves of C 3 species, *planta*, *149*(1), 78-90.https://doi.org/10.1007/BF00386231.

Fensholt, R., T. Langanke, K. Rasmussen, A. Reenberg, S. D. Prince, C. Tucker, et al. (2012), Greenness in semi-arid areas across the globe 1981–2007—an Earth Observing Satellite based analysis of trends and drivers, *Remote sensing of environment*, *121*, 144-158.https://doi.org/10.1016/j.rse.2012.01.017.

Field, C. B., R. B. Jackson, and H. A. Mooney (1995), Stomatal responses to increased CO2: implications from the plant to the global scale, *Plant, Cell & Environment*, *18*(10), 1214-1225.https://doi.org/10.1111/j.1365-3040.1995.tb00630.x.

Forbes, W. L., J. Mao, M. Jin, S.-C. Kao, W. Fu, X. Shi, et al. (2018), Contribution of environmental forcings to US runoff changes for the period 1950–2010, *Environmental Research Letters*, *13*(5), 054023.https://doi.org/10.1088/1748-9326/aabb41.

Frank, D., B. Poulter, M. Saurer, J. Esper, C. Huntingford, G. Helle, et al. (2015), Water-use efficiency and transpiration across European forests during the Anthropocene, *Nature Climate Change*, *5*(6), 579-583.https://doi.org/10.1038/nclimate2614.

Goeking, S. A., and D. G. Tarboton (2020), Forests and water yield: A synthesis of disturbance effects on streamflow and snowpack in western coniferous forests, *J. For.*, *118*(2), 172-192.https://doi.org/10.1093/jofore/fvz069.

Hamlet, A. F., and D. P. Lettenmaier (1999), Effects of climate change on hydrology and water resources in the Columbia River Basin 1, *JAWRA Journal of the American Water Resources Association*, *35*(6), 1597-1623.https://doi.org/10.1111/j.1752-1688.1999.tb04240.x.

Hamlet, A. F., P. W. Mote, M. P. Clark, and D. P. Lettenmaier (2007), Twentieth-century trends in runoff, evapotranspiration, and soil moisture in the western United States, *Journal of Climate*, *20*(8), 1468-1486.https://doi.org/10.1175/JCLI4051.1.

Hicke, J. A., A. J. Meddens, and C. A. Kolden (2016), Recent tree mortality in the western United States from bark beetles and forest fires, *For. Sci.*, *62*(2), 141-153.https://doi.org/10.5849/forsci.15-086.

Huang, R., X. Chen, and Q. Hu (2019), Changes in vegetation and surface water balance at basin-scale in Central China with rising atmospheric CO 2, *Climatic Change*, *155*(3), 437-454.https://doi.org/10.1007/s10584-019-02475-w.

Idso, S., and A. Brazel (1984), Rising atmospheric carbon dioxide concentrations may increase streamflow, *Nature*, *312*(5989), 51-53.https://doi.org/10.1038/312051a0.

Jiang, X., S. A. Rauscher, T. D. Ringler, D. M. Lawrence, A. P. Williams, C. D. Allen, et al. (2013), Projected future changes in vegetation in western North America in the twenty-first century, *Journal of Climate*, *26*(11), 3671-3687.https://doi.org/10.1175/JCLI-D-12-00430.1.

Jung, M., M. Reichstein, H. A. Margolis, A. Cescatti, A. D. Richardson, M. A. Arain, et al. (2011), Global patterns of land-atmosphere fluxes of carbon dioxide, latent heat, and sensible heat derived from eddy covariance, satellite, and meteorological observations, *Journal of Geophysical Research: Biogeosciences*, *116*(G3).https://doi.org/10.1029/2010JG001566.

Kennedy, D., S. Swenson, K. W. Oleson, D. M. Lawrence, R. Fisher, A. C. Lola da Costa, and P. Gentine (2019), Implementing plant hydraulics in the community land model, version 5, *Journal of Advances in Modeling Earth Systems*, *11*(2), 485-513.https://doi.org/10.1029/2018MS001500.

Landerer, F. W., and S. Swenson (2012), Accuracy of scaled GRACE terrestrial water storage estimates, *Water resources research*, *48*(4). https://doi.org/10.1029/2011WR011453.

Lemordant, L., P. Gentine, A. S. Swann, B. I. Cook, and J. Scheff (2018), Critical impact of vegetation physiology on the continental hydrologic cycle in response to increasing CO2, *Proceedings of the National Academy of Sciences*, *115*(16), 4093-4098.https://doi.org/10.1073/pnas.1720712115.

Li, L., Z. L. Yang, A. M. Matheny, H. Zheng, S. C. Swenson, D. M. Lawrence, et al. (2021), Representation of Plant Hydraulics in the Noah-MP Land Surface Model: Model Development and Multi-scale Evaluation, *Journal of Advances in Modeling Earth Systems*, e2020MS002214.https://doi.org/10.1029/2020MS002214.

Lian, X., S. Piao, C. Huntingford, Y. Li, Z. Zeng, X. Wang, et al. (2018), Partitioning global land evapotranspiration using CMIP5 models constrained by observations, *Nature Climate Change*, *8*(7), 640-646.https://doi.org/10.1038/s41558-018-0207-9.

Liu, Y., A. J. Parolari, M. Kumar, C.-W. Huang, G. G. Katul, and A. Porporato (2017), Increasing atmospheric humidity and CO2 concentration alleviate forest mortality risk, *Proceedings of the National Academy of Sciences*, *114*(37), 9918-9923.https://doi.org/10.1073/pnas.1704811114.

Ma, N., G. Y. Niu, Y. Xia, X. Cai, Y. Zhang, Y. Ma, and Y. Fang (2017), A systematic evaluation of Noah-MP in simulating land-atmosphere energy, water, and carbon exchanges over the continental United States, *J. Geophys. Res. Atmos.*, *122*(22), 12,245-212,268.https://doi.org/10.1002/2017JD027597.

Mahowald, N., F. Lo, Y. Zheng, L. Harrison, C. Funk, D. Lombardozzi, and C. Goodale (2016), Projections of leaf area index in earth system models, *Earth System Dynamics (Online)*, *7*(1).https://doi.org/10.5194/esd-7-211-2016.

Mankin, J. S., J. E. Smerdon, B. I. Cook, A. P. Williams, and R. Seager (2017), The curious case of projected twenty-first-century drying but greening in the American West, *Journal of Climate*, *30*(21), 8689-8710.https://doi.org/10.1175/JCLI-D-17-0213.1.

Mankin, J. S., R. Seager, J. E. Smerdon, B. I. Cook, and A. P. Williams (2019), Mid-latitude freshwater availability reduced by projected vegetation responses to climate change, *Nature Geoscience*, *12*(12), 983-988.https://doi.org/10.1038/s41561-019-0480-x.

Mao, J., X. Shi, P. E. Thornton, F. M. Hoffman, Z. Zhu, and R. B. Myneni (2013), Global latitudinal-asymmetric vegetation growth trends and their driving mechanisms: 1982–2009, *Remote Sensing*, *5*(3), 1484-1497.https://doi.org/10.3390/rs5031484.

Milly, P. C., and K. A. Dunne (2016), Potential evapotranspiration and continental drying, *Nature Climate Change*, *6*(10), 946-949.https://doi.org/10.1038/nclimate3046.

Milly, P. C., and K. A. Dunne (2020), Colorado River flow dwindles as warming-driven loss of reflective snow energizes evaporation, *Science*, *367*(6483), 1252-1255.https://doi.org/10.1126/science.aay9187.

Monteith, J. L. (1965), Evaporation and environment, paper presented at Symposia of the society for experimental biology, Cambridge University Press (CUP) Cambridge.

Mueller, B., S. I. Seneviratne, C. Jimenez, T. Corti, M. Hirschi, G. Balsamo, et al. (2011), Evaluation of global observations-based evapotranspiration datasets and IPCC AR4 simulations, *Geophysical Research Letters*, *38*(6).https://doi.org/10.1029/2010GL046230.

Naz, B. S., S.-C. Kao, M. Ashfaq, D. Rastogi, R. Mei, and L. C. Bowling (2016), Regional hydrologic response to climate change in the conterminous United States using high-resolution hydroclimate simulations, *Global and Planetary Change*, *143*, 100-117.https://doi.org/10.1016/j.gloplacha.2016.06.003.

Neto, A. A. M., G.-Y. Niu, T. Roy, S. Tyler, and P. A. Troch (2020), Interactions between snow cover and evaporation lead to higher sensitivity of streamflow to temperature, *Communications Earth & Environment*, *1*(1), 1-7.https://doi.org/10.1038/s43247-020-00056-9.

Niu, G. Y., Z. L. Yang, R. E. Dickinson, L. E. Gulden, and H. Su (2007), Development of a simple groundwater model for use in climate models and evaluation with Gravity Recovery and Climate Experiment data, *Journal of Geophysical Research: Atmospheres*, *112*(D7).https://doi.org/10.1029/2006JD007522.

Niu, G. Y., Y. H. Fang, L. L. Chang, J. Jin, H. Yuan, and X. Zeng (2020), Enhancing the Noah-MP Ecosystem Response to Droughts with an Explicit Representation of Plant Water Storage Supplied by Dynamic Root Water Uptake, *Journal of Advances in Modeling Earth Systems*, e2020MS002062.https://doi.org/10.1029/2020MS002062.

Niu, G. Y., Z. L. Yang, K. E. Mitchell, F. Chen, M. B. Ek, M. Barlage, et al. (2011), The community Noah land surface model with multiparameterization options (Noah-MP): 1. Model description and evaluation with local-scale measurements, *J. Geophys. Res. Atmos.*, *116*(D12).https://doi.org/10.1029/2010JD015139.

Parton, W., J. Singh, and D. Coleman (1978), A model of production and turnover of roots in shortgrass prairie, *Journal of Applied Ecology*, 515-541.https://doi.org/10.2307/2402608.

Prather, M., G. Flato, P. Friedlingstein, C. Jones, J. Lamarque, H. Liao, and P. Rasch (2013), Annex II: Climate system scenario tables, *Climate change*, 1395-1445

Roderick, M. L., P. Greve, and G. D. Farquhar (2015), On the assessment of aridity with changes in atmospheric CO2, *Water Resources Research*, *51*(7), 5450-5463.https://doi.org/10.1002/2015WR017031.

Sakumura, C., S. Bettadpur, and S. Bruinsma (2014), Ensemble prediction and intercomparison analysis of GRACE time-variable gravity field models, *Geophysical Research Letters*, *41*(5), 1389-1397.https://doi.org/10.1002/2013GL058632.

Singh, A., S. Kumar, S. Akula, D. M. Lawrence, and D. L. Lombardozzi (2020), Plant growth nullifies the effect of increased water-use efficiency on streamflow under elevated CO2 in the Southeastern United States, *Geophysical Research Letters*, *47*(4), e2019GL086940.https://doi.org/10.1029/2019GL086940.

Smith, W. K., S. C. Reed, C. C. Cleveland, A. P. Ballantyne, W. R. Anderegg, W. R. Wieder, et al. (2016), Large divergence of satellite and Earth system model estimates of global terrestrial CO 2 fertilization, *Nature climate change*, *6*(3), 306-310.https://doi.org/10.1038/nclimate2879.

Sun, S., G. Sun, E. C. Mack, S. McNulty, P. V. Caldwell, K. Duan, and Y. Zhang (2016), Projecting water yield and ecosystem productivity across the United States by linking an ecohydrological model to WRF dynamically downscaled climate data, *Hydrology and Earth System Sciences*, *20*(2), 935-952.https://doi.org/10.5194/hess-20-935-2016.

Swann, A. L., F. M. Hoffman, C. D. Koven, and J. T. Randerson (2016), Plant responses to increasing CO2 reduce estimates of climate impacts on drought severity, *Proceedings of the National Academy of Sciences*, *113*(36), 10019-10024.https://doi.org/10.1073/pnas.1604581113.

Taylor, K. E., R. J. Stouffer, and G. A. Meehl (2012), An overview of CMIP5 and the experiment design, *Bull. Amer. Meteor. Soc.*, *93*(4), 485-498.https://doi.org/10.1175/BAMS-D-11-00094.1.

Thorne, J. H., H. Choe, P. A. Stine, J. C. Chambers, A. Holguin, A. C. Kerr, and M. W. Schwartz (2018), Climate change vulnerability assessment of forests in the Southwest USA, *Climatic Change*, *148*(3), 387-402.https://doi.org/10.1007/s10584-017-2010-4.

Ukkola, A., T. Keenan, D. I. Kelley, and d. I. Prentice (2016), Vegetation plays an important role in mediating future water resources, *Environmental Research Letters*, *11*(9), 094022.https://doi.org/10.1088/1748-9326/11/9/094022.

name not right

Vose, R., D. R. Easterling, K. Kunkel, and M. Wehner (2017), Temperature changes in the United States.https://doi.org/10.7930/J0N29V45.

which journal

Xia, Y., K. Mitchell, M. Ek, J. Sheffield, B. Cosgrove, E. Wood, et al. (2012), Continental-scale water and energy flux analysis and validation for the North American Land Data Assimilation System project phase 2 (NLDAS-2): 1. Intercomparison and application of model products, *Journal of Geophysical Research: Atmospheres*, *117*(D3).https://doi.org/10.1029/2011JD016048.

Xue, Y., Z. Janjic, J. Dudhia, R. Vasic, and F. De Sales (2014), A review on regional dynamical downscaling in intraseasonal to seasonal simulation/prediction and major factors that affect downscaling ability, *Atmos. Res.*, *147*, 68-85.https://doi.org/10.1016/j.atmosres.2014.05.001.

Yan, K., T. Park, G. Yan, Z. Liu, B. Yang, C. Chen, et al. (2016), Evaluation of MODIS LAI/FPAR product collection 6. Part 2: Validation and intercomparison, *Remote Sens.*, *8*(6), 460.https://doi.org/10.3390/rs8060460.

Yang, Y., R. J. Donohue, T. R. McVicar, M. L. Roderick, and H. E. Beck (2016), Long-term CO2 fertilization increases vegetation productivity and has little effect on hydrological partitioning in tropical rainforests, *Journal of Geophysical Research: Biogeosciences*, *121*(8), 2125-2140.https://doi.org/10.1002/2016JG003475.

Yang, Y., M. L. Roderick, S. Zhang, T. R. McVicar, and R. J. Donohue (2019), Hydrologic implications of vegetation response to elevated CO 2 in climate projections, *Nature Climate Change*, *9*(1), 44-48.https://doi.org/10.1038/s41558-018-0361-0.

Yang, Z. L., G. Y. Niu, K. E. Mitchell, F. Chen, M. B. Ek, M. Barlage, et al. (2011), The community Noah land surface model with multiparameterization options (Noah-MP): 2. Evaluation over global river basins, *Journal of Geophysical Research: Atmospheres*, *116*(D12). https://doi.org/10.1029/2010JD015140.

Yuan, H., Y. Dai, Z. Xiao, D. Ji, and W. Shangguan (2011), Reprocessing the MODIS Leaf Area Index products for land surface and climate modelling, *Remote Sensing of Environment*, *115*(5), 1171-1187.https://doi.org/10.1016/j.rse.2011.01.001.

Zeng, X., P. Broxton, and N. Dawson (2018), Snowpack change from 1982 to 2016 over conterminous United States, *Geophysical Research Letters*, *45*(23), 12,940-912,947. https://doi.org/10.1029/2018GL079621.

Zeng, Z., L. Peng, and S. Piao (2018), Response of terrestrial evapotranspiration to Earth's greening, *Current opinion in environmental sustainability*, *33*, 9-25.https://doi.org/10.1016/j.cosust.2018.03.001.

Zeng, Z., S. Piao, L. Z. Li, L. Zhou, P. Ciais, T. Wang, et al. (2017), Climate mitigation from vegetation biophysical feedbacks during the past three decades, *Nature Climate Change*, *7*(6), 432-436.https://doi.org/10.1038/nclimate3299.

Zheng, H., Z. L. Yang, P. Lin, W. Y. Wu, L. Li, Z. Xu, et al. (2020), Falsification-oriented signature-based evaluation for guiding the development of land surface models and the enhancement of observations, *Journal of Advances in Modeling Earth Systems*, *12*(12), e2020MS002132.https://doi.org/10.1029/2020MS002132.

Zhu, Q., W. J. Riley, J. Tang, N. Collier, F. M. Hoffman, X. Yang, and G. Bisht (2019), Representing nitrogen, phosphorus, and carbon interactions in the E3SM land model: Development and global benchmarking, *Journal of Advances in Modeling Earth Systems*, *11*(7), 2238-2258.https://doi.org/10.1029/2018MS001571.

Zhu, S., H. Chen, X. Zhang, N. Wei, W. Shangguan, H. Yuan, et al. (2017), Incorporating root hydraulic redistribution and compensatory water uptake in the Common Land Model: Effects on site level and global land modeling, *Journal of Geophysical Research: Atmospheres*, *122*(14), 7308-7322.https://doi.org/10.1002/2016JD025744.

Zhu, Z., S. Piao, X. Lian, R. B. Myneni, S. Peng, and H. Yang (2017), Attribution of seasonal leaf area index trends in the northern latitudes with “optimally” integrated ecosystem models, *Glob. Chang. Biol.*, *23*(11), 4798-4813.https://doi.org/10.1111/gcb.13723.